Magnetic exchange coupling in cuprate-analog d^9 nickelates

Yusuke Nomura [1,*] Takuya Nomoto [2] Motoaki Hirayama [1] and Ryotaro Arita [1,2]
[1]*RIKEN Center for Emergent Matter Science, 2-1 Hirosawa, Wako, Saitama 351-0198, Japan*
[2]*Department of Applied Physics, University of Tokyo,7-3-1 Hongo, Bunkyo-ku, Tokyo 113-8656*

(Received 30 June 2020; revised 28 September 2020; accepted 29 September 2020; published 27 October 2020)

Motivated by the recent discovery of superconductivity in doped $NdNiO_2$, we study the magnetic exchange interaction J in layered d^9 nickelates from first principles. The mother compounds of the high-T_c cuprates belong to the charge-transfer regime in the Zaanen-Sawatzky-Allen diagram and have J larger than 100 meV. While this feature makes the cuprates very different from other transition metal oxides, it is of great interest whether layered d^9 nickelates can also have such a large J. However, one complexity is that $NdNiO_2$ is not a Mott insulator due to carrier doping from the block layer. To compare the cuprates and d^9 nickelates on an equal basis, we study $RbCa_2NiO_3$ and $A_2NiO_2Br_2$ (A denotes a cation with a valence of 2.5+), which were recently designed theoretically by block-layer engineering. These nickelates are free from the self-doping effect and belong to the Mott-Hubbard regime. We show that these nickelates share a common thread with the high-T_c cuprates in that they also have a significant exchange interaction J as large as about 100 meV.

DOI: 10.1103/PhysRevResearch.2.043144

I. INTRODUCTION

The discovery of superconductivity in doped nickel oxides $Nd_{0.8}Sr_{0.2}NiO_2$ [1,2] has attracted intensive interest in both experiment [3–13] and theory [3,14–52] because the nickelate might be an analog of the well-known high-T_c superconductor, cuprates. Recently, the doping dependence has been explored both theoretically [37] and experimentally [8,9] and the presence of the superconducting dome has been confirmed [8,9]. The maximum superconducting transition temperature T_c is about 15 K, not very high compared to that of the high-T_c cuprates. However, because the Bardeen-Cooper-Schrieffer phonon mechanism cannot explain the observed T_c [17], the superconducting mechanism is most likely unconventional, in which the electron correlations play an important role [15,25,37,51]. A recent observation of a d-wave-like superconducting gap also supports this scenario [12]. Here a natural question arises: Is there any possibility to realize T_c as high as for the cuprates in nickelates?

In the cuprates, the superconductivity emerges by doping carriers into the antiferromagnetic Mott insulator having a large magnetic exchange coupling J ($\sim$130 meV) [53]. One of the reasons for the large J is because the cuprates belong to the charge-transfer type in the Zaanen-Sawatzky-Allen diagram [54]; in addition, the charge-transfer energy Δ_{dp} (the energy difference between the copper $3d$ and oxygen $2p$ orbitals) is small among transition metal oxides. Although the mechanism of the high-T_c superconductivity is highly controversial, the large J is a plausible factor in enhancing the d-wave superconductivity in the cuprates.[1] This large value of J is certainly a characteristic feature of the cuprates, which makes the cuprates very different from other transition metal oxides.

On the other hand, in the case of the nickelate $NdNiO_2$, Δ_{dp} is larger than that of the cuprates [56]. Thus, we naively expect smaller J for nickelates. Indeed, a recent experimental estimate using the Raman spectroscopy gives $J = 25$ meV [6]. However, it should be noted that the origin of small J in $NdNiO_2$ may be ascribed to another notable difference from the cuprates, namely, $NdNiO_2$ is not a Mott insulator due to the self-doping effect. In $NdNiO_2$, orbitals in the Nd layer form extra Fermi pockets on top of the large Fermi surface formed by the Ni $3d_{x^2-y^2}$ orbital and the Ni $3d_{x^2-y^2}$ orbital is hole doped, i.e., the filling of the Ni $3d$ orbitals deviates from d^9 [14,15,19,33,49,56]. The self-doping naturally explains the absence of Mott insulating behavior in $NdNiO_2$. Although it has been shown that the Ni $3d_{x^2-y^2}$ orbital forms a two-dimensional strongly correlated system [17], J at the d^9 configuration with a half-filled $d_{x^2-y^2}$ orbital is masked by the self-doping. The experimental estimate should be understood as the J value including the effect of the self-doping, not the J value at the ideal d^9 configuration. One of the reasons for the controversy in theory about the size of J [20–29] is ascribed to the ambiguity in calculating J (whether we calculate J at d^9 filling or J including the self-doping effect). In any case, it is a nontrivial problem whether we can justify the mapping onto a simple spin model to understand the property of $NdNiO_2$. This fact makes $NdNiO_2$ an imperfect analog of the cuprates.

*yusuke.nomura@riken.jp

[1]For example, in the t-J model, the superconducting transition temperature scales with J. For details, see, e.g., Refs. [53,55].

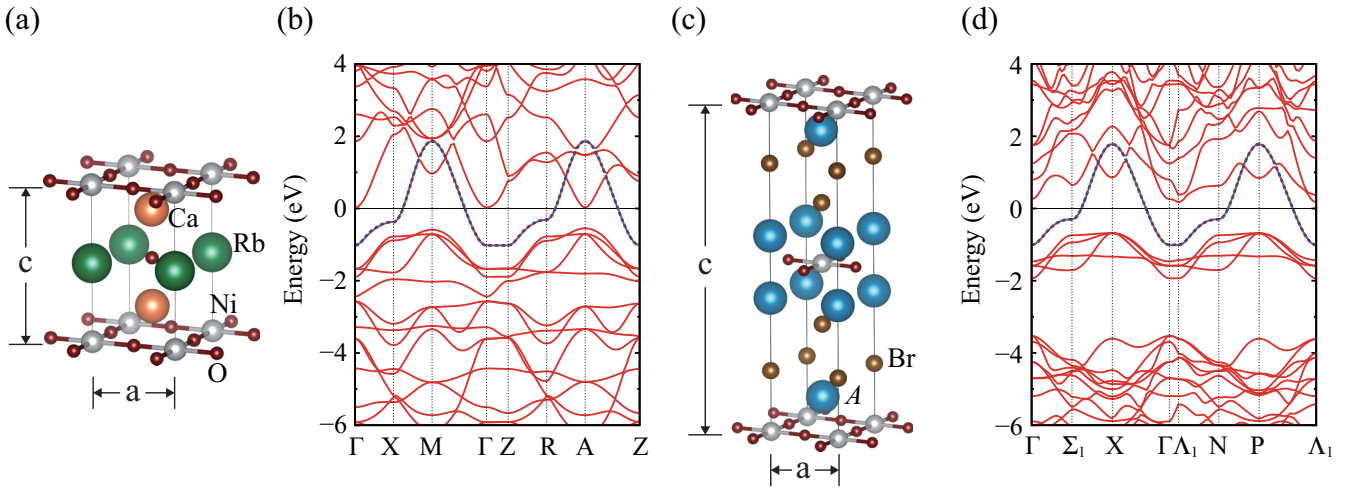

FIG. 1. Crystal structure of (a) $RbCa_2NiO_3$ and (c) $A_2NiO_2Br_2$ (A denotes a cation with a valence of 2.5+) and the paramagnetic DFT band structure of (b) $RbCa_2NiO_3$ and (d) $A_2NiO_2Br_2$ (A denotes $Ba_{0.5}La_{0.5}$). The blue dotted curves are the Wannier band dispersion of the Ni $3d_{x^2-y^2}$ single-orbital Hamiltonian. In (b) and (d), the consistent **k** path is employed: $(0, 0, 0) \to (\pi/a, 0, 0) \to (\pi/a, \pi/a, 0) \to (0, 0, 0) \to (0, 0, \pi/c) \to (\pi/a, 0, \pi/c) \to (\pi/a, \pi/a, \pi/c) \to (0, 0, \pi/c)$ (the symbols are different because the primitive cells of $RbCa_2NiO_3$ and $A_2NiO_2Br_2$ are tetragonal and base-centered tetragonal, respectively).

Recently, there was a proposal to design cuprate-analog nickelates without the complication of the self-doping [18].[2] Since $NdNiO_2$ is a layered material, one can systematically propose nickelate family materials by changing the composition of the block layer [57] between NiO_2 layers. Proposed dynamically stable nickelates have smaller Fermi pockets of the block-layer orbitals than $NdNiO_2$. In some materials, the self-doping is completely suppressed and the ideal d^9 system with half-filled $3d_{x^2-y^2}$ orbital is realized. An *ab initio* estimate of Hubbard U using the constrained random-phase approximation (cRPA) [58] shows that the correlation strength U/t (t denotes nearest-neighbor hopping) is comparable to that of cuprates [18]. Therefore, once such nickelates are synthesized, the mother compounds will be a Mott insulator similarly to the cuprates and the effective model becomes the Heisenberg model, which gets rid of the ambiguity in calculating J.

In this paper, we study the strength of J in the two ideal d^9 nickelates, which are free from the self-doping (see Sec. II for the details of the materials). We estimate the J value by the following three methods [59]. First, we start from a single-orbital Hubbard model derived in Ref. [18] and then evaluate J by the expansion in terms of t/U. Second, we perform an energy mapping between the classical Heisenberg model and the total energy of different magnetic configurations calculated by a method using the local-density approximation plus Hubbard-type Coulomb interactions (LDA+U). Third, we employ a scheme based on the so-called local force theorem. Hereafter, we simply call these three methods strong-coupling expansion, energy mapping method, and local force approach, respectively. We show that the three independent estimates show reasonable agreement and conclude that the d^9 nickelates have a sizable J (about 100 meV), which is not far smaller than that of the cuprates. Therefore, the proposed d^9 nickelates provide an interesting playground to explore the cuprate-analog high-T_c superconductivity.

The paper is organized as follows. In Sec. II we introduce two ideal d^9 nickelates $RbCa_2NiO_3$ and $A_2NiO_2Br_2$ (A denotes a cation with a valence of 2.5+) and discuss the advantage over $NdNiO_2$. In Sec. III we explain the three methods employed in the present study. We show the results in Sec. IV. Section V is devoted to a summary.

II. MATERIALS: d^9 NICKELATES

In Ref. [18], various layered nickelates have been systematically proposed. They are classified into 1213, 1214, H_2, and G families, depending on the composition and the type of block layer [57]. Among the four families, the compounds without the self-doping exist in the 1213 and G families. We here take $RbCa_2NiO_3$ and $A_2NiO_2Br_2$ (again A denotes a cation with a valence of 2.5+) for a representative of the ideal d^9 nickelates belonging to 1213 and G families, respectively [see Figs. 1(a) and 1(c) for the crystal structure]. In the following, we employ $Ba_{0.5}La_{0.5}$ as A. The phonon calculations have shown that both $RbCa_2NiO_3$ and $A_2NiO_2Br_2$ ($A = Ba_{0.5}La_{0.5}$) are dynamically stable [18]. We take the crystal structure optimized in Ref. [18] and perform density-functional theory (DFT) calculations.[3] Figures 1(b) and 1(d) show the paramagnetic DFT band structure for $RbCa_2NiO_3$ and $A_2NiO_2Br_2$ ($A = Ba_{0.5}La_{0.5}$), respectively. As shown in Ref. [18], only the Ni $3d_{x^2-y^2}$ orbital crosses the Fermi level. As far as the topology of the band structure is concerned, these systems are more similar to the cuprates than $NdNiO_2$.

[2] See also Refs. [48,52] for other attempts to find nickelate superconductors.

[3] Here we ignore the interface effect [45–47] and consider the bulk property. Note that the thickness of the film reaches around 10 nm and there are several tens of NiO_2 layers in the sample [7].

The advantages of studying these nickelates rather than $NdNiO_2$ are as follows. First, it is still controversial whether the role of Nd-layer (block-layer) orbitals is essential or not. If the hybridization between Ni $3d$ and Nd-layer orbitals is substantial, the Nd-layer orbitals not only are a charge reservoir, but they might give Kondo-like physics [2,3,23,32,42]. In the cases of the d^9 nickelates $RbCa_2NiO_3$ and $A_2NiO_2Br_2$ ($A = Ba_{0.5}La_{0.5}$), the block-layer orbitals do not show up at the Fermi level and this controversy can be avoided. We can also exclude the possible role of the $4f$ orbitals with localized moments proposed in Refs. [43,44].

Another controversial issue for $NdNiO_2$ is to which orbitals the doped holes go ($d^9\underline{L}$ vs d^8, where $\underline{L}$ denotes a hole in a ligand oxygen). In the case of the cuprates (charge-transfer insulator), the holes are doped into the oxygen $2p$ orbitals. On the other hand, the nickelates have larger Δ_{dp} and are classified as Mott-Hubbard type [3,6,10,17,20,22]. Because there is nonzero hybridization between Ni $3d_{x^2-y^2}$ and O $2p$ orbitals, some of the holes should be doped into oxygen $2p$ orbitals [16,27,36]. However, the amount should be smaller than that of the cuprates.

When the system is of Mott-Hubbard type and the holes mainly reside in the Ni $3d$ orbitals, another issue arises: Which model is more appropriate, the single-orbital or multiorbital model? In other words, does the doped d^8 configuration favor the high-spin state or the low-spin state. If the crystal field splitting between Ni $3d_{x^2-y^2}$ and the other $3d$ orbitals is much larger than the Hund's coupling, holes stay within the Ni $3d_{x^2-y^2}$ orbital and the single-orbital model is justified. On this issue, several studies insist that Ni $3d$ multiorbital nature cannot be ignored [20,30,31,34,35,38–41,50]. To resolve this issue, we certainly need more experimental evidence. In the cases of $RbCa_2NiO_3$ and $A_2NiO_2Br_2$ ($A = Ba_{0.5}La_{0.5}$), compared to $NdNiO_2$, the Ni $3d_{x^2-y^2}$ orbital is more isolated in energy space from the other $3d$ orbitals [see Figs. 1(b) and 1(d)]: In the case of $NdNiO_2$, due to the dispersion in the k_z direction, the position of the Ni $d_{3z^2-r^2}$ band becomes close to the Fermi level on the $k_z = \pi/c$ plane; however, such a k_z dependence is much weaker in $RbCa_2NiO_3$ and $A_2NiO_2Br_2$ ($A = Ba_{0.5}La_{0.5}$). Considering also the above-mentioned absence of the complication from the self-doping, in this study, we adopt the single-orbital Hubbard model as a minimal model for $RbCa_2NiO_3$ and $A_2NiO_2Br_2$ ($A = Ba_{0.5}La_{0.5}$). In the absence of the carrier doping, we can further map onto the spin model with the exchange coupling J.

III. METHODS

Here we introduce three different methods to estimate J (see, e.g., Ref. [59] for the ideas behind the three methods). We employ the following convention for the spin Hamiltonian: $\mathcal{H} = \sum_{\langle i,j\rangle} J_{ij}\mathbf{S}_i \cdot \mathbf{S}_j$, where $\langle i, j\rangle$ is the bond consisting of sites i and j and $\mathbf{S}_i$ is the spin-1/2 operator at site i. Here J stands for the nearest-neighbor J_{ij} interaction in the NiO_2 layer.

A. Strong-coupling expansion

When the single-orbital Hubbard model is a good description, the magnetic interactions in the Mott insulating region can be obtained by strong-coupling perturbation expansion. The strong-coupling expansion becomes valid in the region $U \gtrsim W$ with the bandwidth W (in the square lattice $W = 8t$) [60]. $RbCa_2NiO_3$ and $A_2NiO_2Br_2$ ($A = Ba_{0.5}La_{0.5}$) with $U/t = 9.522$ and 10.637, respectively [18], satisfy the condition $U > W$.

In the strong-coupling expansion, the superexchange interaction J_s (with t^4-order correction term) and cyclic ring-exchange interaction J_c are given by $J_s = 4t^2/U - 24t^4/U^3$ and $J_c = 80t^4/U^3$, respectively [61–63]. If we effectively take into account the effect of the ring-exchange interaction in the nearest-neighbor interaction J, the J value becomes

$$J = J_s - 2J_cS^2 = \frac{4t^2}{U} - \frac{64t^4}{U^3}, \tag{1}$$

with $S = 1/2$.

B. Energy mapping method

Within the LDA+U [64–67], we perform the magnetic calculations. Here U is introduced into the Ni $3d$ orbital subspace. We employ a $2 \times 2 \times 1$ supercell consisting of four conventional cells. We simulate two different magnetic solutions: One is Néel type [$(\pi/a, \pi/a, 0)$ antiferromagnetic order] and the other is stripe type [$(\pi/a, 0, 0)$ antiferromagnetic order]. We calculate the energy difference ΔE between the two antiferromagnetic solutions. When we assume the two-dimensional classical spin-1/2 Heisenberg model up to next-nearest-neighbor magnetic interaction J', ΔE per formula unit is given by $\Delta E = J/2 - J' \simeq J/2$. We estimate J with this equation.

C. Local force approach

Based on the Néel-type solutions of the LDA+U calculations, we estimate J and J' using the local force theorem [59]. The local force approach estimates the magnetic interactions from the small energy change induced by the infinitesimal spin rotation from the magnetic solutions (Néel type in the present case). We employ the so-called Liechtenstein formula, which was developed in the low-energy Hamiltonian with the Wannier orbitals [68–70], given by

$$(-1)^P J_{ij} = 4T \sum_{\omega_n} \mathrm{Tr}[G_{ij}(\omega_n)M_jG_{ji}(\omega_n)M_i], \tag{2}$$

where $\omega_n = (2n+1)\pi T$ denotes the Matsubara frequency. Here we set $P = 0$ (1) when the spins at i and j sites are aligned parallel (antiparallel) to each other. The Green's function G_{ij} is defined by $G_{ij}^{-1}(i\omega_n) = (i\omega_n + \mu)\delta_{ij} - \mathcal{H}^0_{ij}$, where $\mathcal{H}^0_{ij}$ is the hopping matrix of the Wannier tight-binding model and μ is the chemical potential. Note that $\mathcal{H}^0_{ij}$ is an $N_{\mathrm{orb}_i} \times N_{\mathrm{orb}_j}$ matrix, where N_{orb_i} is the number of Wannier orbitals at the i site including the spin index. In the case of collinear magnets, one may write $\mathcal{H}^0_{ii}$ as $\mathcal{H}^0_{ii} = \varepsilon_i \otimes \sigma_0 + m_i \otimes \sigma_z$. Then M_i is defined by $M_i = m_i \otimes \sigma_x$ and is proportional to the exchange splitting at the i site m_i. Here we have neglected the spin-dependent hopping term of M_i (see Ref. [69] for details[4]).

[4]Note that the J_{ij} value in this paper is defined to be eight times as large as that in Ref. [69].

D. Comparison among the three methods

The strong-coupling expansion gives local (in real space) J, the energy mapping method sees the energy difference between the global and local minima of the magnetic solutions, and the local force method sees the low-energy excitations around the global minimum. These J are complementary to each other, and hence we employ all three methods. When the Coulomb repulsion is much larger than the bandwidth and the mapping to the Heisenberg model becomes valid, these three methods see the same J. As we will show in Sec. IV, the three results agree reasonably well, as expected from the Mott insulating behavior of the proposed d^9 nickelates.

E. Calculation conditions

The DFT band structure calculations are performed using QUANTUM ESPRESSO [71]. We employ Perdew-Burke-Ernzerhof [72] norm-conserving pseudopotentials downloaded from PSEUDODOJO [73] (the pseudopotentials are based on optimized norm-conserving Vanderbilt pseudopotentials [74]).

The energy comparison between the Néel- and stripe-type antiferromagnetic solutions is performed using $9 \times 9 \times 7$ and $9 \times 9 \times 3$ $\mathbf{k}$ meshes for $RbCa_2NiO_3$ and $A_2NiO_2Br_2$ ($A = Ba_{0.5}La_{0.5}$), respectively. We treat $Ba_{0.5}La_{0.5}$ by the virtual crystal approximation. The energy cutoff is set to be 100 Ry for the Kohn-Sham wave functions and 400 Ry for the electron charge density.

For the estimate of J based on the local force approach, we first construct the maximally localized Wannier functions [75,76] for the Néel-type antiferromagnetic band structure using RESPACK [77,78]. For $RbCa_2NiO_3$, we use a $5 \times 5 \times 5$ $\mathbf{k}$ mesh for the construction of Wannier orbitals. We use Ni d, O p, Ca d, and interstitial-s (located at the interstitial positions surrounded by Ni^+, Ca^{2+}, and Rb^+ cations) projections. The interstitial orbitals are stabilized because they experience attraction from the surrounded cations [17]. Then we obtain a 104-orbital (per spin) tight-binding Hamiltonian. For $A_2NiO_2Br_2$ ($A = Ba_{0.5}La_{0.5}$), we employ a $5 \times 5 \times 3$ $\mathbf{k}$ mesh for constructing Wannier orbitals. We derive a 232-orbital (per spin) tight-binding Hamiltonian using the projections of Ni d, O p, Br p, A d, and interstitial-s (located at the interstitial positions surrounded by Ni^+, $A^{2.5+}$, and Br^- ions) orbitals.

In the calculation of Eq. (2), we employ a $16 \times 16 \times 16$ $\mathbf{k}$ mesh and set the inverse temperature $\beta = 200$ eV^{-1} for both cases. We have confirmed that the difference of J_{ij} values at $\beta = 200$ and 400 eV^{-1} is less than 1%. We use the intermediate representation basis for the Matsubara frequency summation [79–81] and set the cutoff parameter $\Lambda = 10^5$, which is sufficiently larger than $W\beta$, where W is the bandwidth.

IV. J IN d^9 NICKELATES

In the previous study [18], the effective single-orbital Hamiltonians for $RbCa_2NiO_3$ and $A_2NiO_2Br_2$ ($A = Ba_{0.5}La_{0.5}$) are constructed using maximally localized Wannier functions [75,76] and the cRPA [58]. The derived nearest-neighbor hopping and Hubbard parameters are $t = -0.352$ eV and $U = 3.347$ eV for $RbCa_2NiO_3$ and $t = -0.337$ eV and $U = 3.586$ eV for $A_2NiO_2Br_2$ ($A = Ba_{0.5}La_{0.5}$). Then the strong-coupling expansion described in Sec. III A gives $J = 122$ and 109 meV for $RbCa_2NiO_3$ and $A_2NiO_2Br_2$ ($A = Ba_{0.5}La_{0.5}$), respectively (see the Appendix for the estimate from the three-orbital d-p model).

Figures 2(a) and 2(b) show the band structure calculated by the LDA+U method for the Néel-type antiferromagnetic state. While the Hubbard U in the single-orbital Hubbard model is the Coulomb repulsion between the Wannier orbitals made from the Ni $3d_{x^2-y^2}$ orbital with O $2p$ tails, the U interaction in the LDA+U calculation is the Coulomb repulsion between the Ni $3d$ orbitals. To make the difference clearer, we call U in the LDA+U calculation $\overline{U}$. In Figs. 2(a) and 2(b), we have used $\overline{U} = 3$ eV.

In contrast to the case of the LDA+U calculation for $NdNiO_2$, where the system stays metallic even in the presence of antiferromagnetic order [14,22,24], both systems become insulating. The top of the valence band has mainly Ni $3d$ character, in agreement with the classification into the Mott-Hubbard-type insulator. We see that both systems are insulating even at smaller $\overline{U}$ (=1 eV). For the whole $\overline{U}$ region we studied (1–5 eV), there exists a well-defined spin-1/2 Ni spin moment. The results suggest that if these d^9 nickelates are synthesized, they become antiferromagnetic Mott insulators as in the cuprates.

Figure 2(c) shows the energy difference ΔE per formula unit between the Néel- and stripe-type antiferromagnetic solutions. The ΔE decreases as $\overline{U}$ increases, which is a natural behavior given that ΔE is governed by J and the origin of J is the superexchange interaction.

In Figs. 2(a) and 2(b), the band dispersions obtained by the Wannier tight-binding Hamiltonian, which are used in the local force approach, are also shown. The Wannier bands well reproduce the LDA+U magnetic band dispersions.

From ΔE in Fig. 2(c), we perform the order estimate of J by the energy mapping method assuming $J'/J = 0.05$ (Sec. III B).[5] Then J is given by $J = \Delta E/0.45$. We also estimate J using the local force approach (Sec. III C).

These results on top of the J value estimated by the strong-coupling expansion (discussed above) are summarized in Figs. 3(a) and 3(b) for $RbCa_2NiO_3$ and $A_2NiO_2Br_2$ ($A = Ba_{0.5}La_{0.5}$), respectively. The J value in the energy mapping method changes from about 140 meV ($\overline{U} = 1$ eV) to 60 meV ($\overline{U} = 5$ eV). The local force approach gives $J \simeq 70$–80 meV. These estimates give the same order of J as the strong-coupling expansion results [$J = 122$ and 109 meV for $RbCa_2NiO_3$ and $A_2NiO_2Br_2$ ($A = Ba_{0.5}La_{0.5}$), respectively].

Although the energy mapping method and local force approach are based on the same LDA+U calculations, we see that there is a discrepancy between the two results at small $\overline{U}$ values (although the difference is no more than two times). It should be noted that the former method sees the global change of the energy between the completely different magnetic patterns, whereas the latter approach only sees the local landscape around the Néel-type solutions, as described in

[5]We do not pay special attention to the precise value of the ratio J'/J because we are only interested in the order estimate of J.

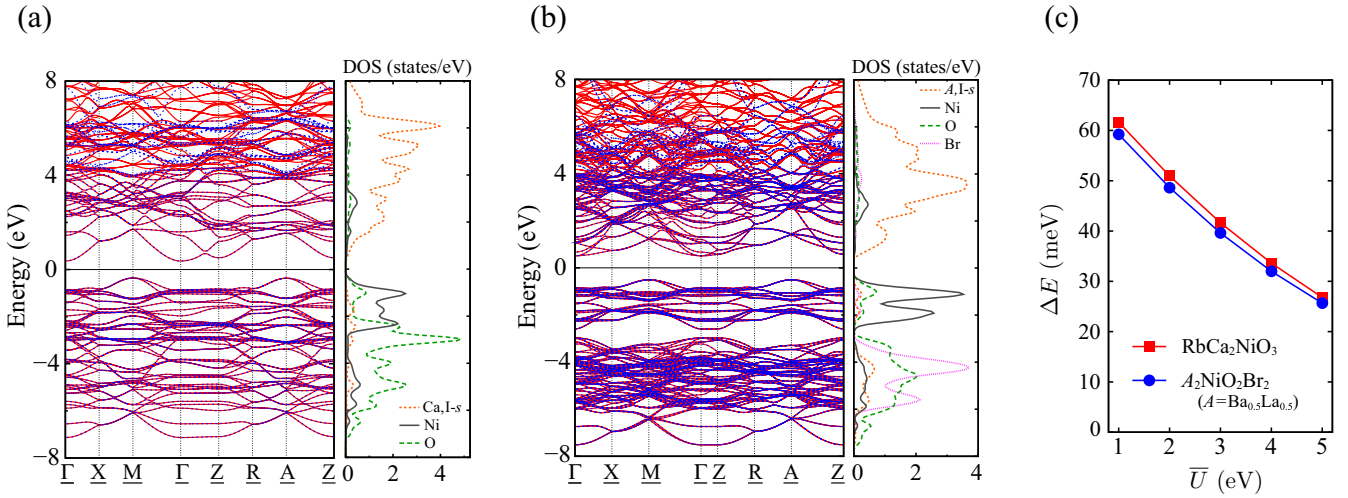

FIG. 2. Néel-type antiferromagnetic band structure (red curves) and orbital-resolved density of states (per formula unit, per spin) for (a) $RbCa_2NiO_3$ and (b) $A_2NiO_2Br_2$ (A denotes $Ba_{0.5}La_{0.5}$), calculated with the LDA+U method ($\overline{U} = 3$ eV). The blue dotted curves are the band dispersion calculated from the Wannier tight-binding Hamiltonian. The symbols for the high-symmetry $\mathbf{k}$ points with the underlines are defined based on a $2 \times 2 \times 1$ supercell consisting of four conventional cells. The origin of the energy axis is set to be the middle of the gap. The orbital-resolved density of states is calculated from the Wannier tight-binding Hamiltonian. Here I-s stands for the interstitial-s orbitals (see Sec. III E for the details of the projections used in the Wannier construction). (c) Energy difference ΔE per formula unit between Néel- and stripe-type antiferromagnetic solutions. The Néel-type solutions always show lower energy.

Sec. III D. For larger $\overline{U}$, the agreement between these two results becomes better, as expected: The system can be mapped to the classical spin model with a constant J regardless of the assumed magnetic structure in the local force approach.

Overall, all three estimates of J lie within 60–140 meV and we conclude that the d^9 nickelates have a sizable J of the order of 100 meV. The agreement in the order estimate of J among three independent methods shows that $RbCa_2NiO_3$ and $A_2NiO_2Br_2$ ($A = Ba_{0.5}La_{0.5}$) are indeed Mott insulators, with the effective model being the Heisenberg model, and the magnetic exchange coupling J is governed by the superexchange interaction [if the materials were, for example, weakly correlated, the three methods would not agree well (see Sec. III D)].

Finally, we compare the J value with that of the cuprates. In the cuprates, the magnitude of J is intensively studied by Raman spectroscopy in the early stage [82–84]. The J value for La_2CuO_4 is estimated to be about 130 meV [85]. Systematic investigations have shown that the material dependence of J in the cuprates family is weak [86,87]. The numerical study of the d-p model has also derived J as large as about 130 meV [88]. Compared to the J value of 130 meV for the cuprates, our estimate based on the d-p model giving 90–100 meV (see the Appendix) is small, which is consistent with the fact that Δ_{dp} is larger in the nickelates. However, we note that the J value of about 100 meV is still significant and the d^9 nickelates would serve as interesting cuprate-analog materials.

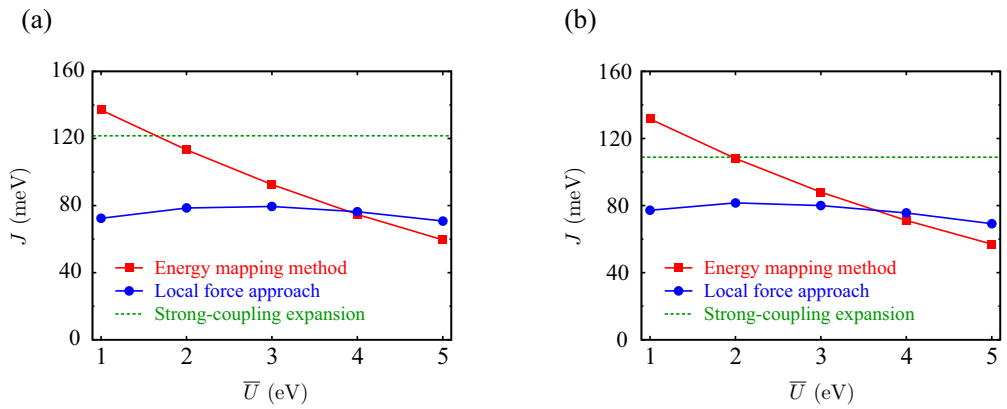

FIG. 3. Estimated exchange coupling J for (a) $RbCa_2NiO_3$ and (b) $A_2NiO_2Br_2$ (A denotes $Ba_{0.5}La_{0.5}$). Here $\overline{U}$ is the Hubbard interaction in the LDA+U calculation (the Coulomb repulsion between the Ni 3d orbitals), which we distinguish from the Hubbard U in the single-orbital Hubbard model used in the strong-coupling expansion (the Coulomb repulsion between the Wannier orbitals made from the Ni $3d_{x^2-y^2}$ orbital with O 2p tails). See the text for details.

V. SUMMARY

One of the remarkable features of the high-T_c cuprates is the large exchange coupling J, whose size is as large as 130 meV [53]. In the present study, we have evaluated the size of J for d^9 nickelates from first principles. While the cuprates having small Δ_{dp} belong to the charge-transfer type in the Zaanen-Sawatzky-Allen diagram [54], nickelates with larger Δ_{dp} belong to the Mott-Hubbard type. To answer how large J can be expected in the Mott-Hubbard insulating d^9 nickelates, we studied $RbCa_2NiO_3$ and $A_2NiO_2Br_2$ ($A = Ba_{0.5}La_{0.5}$), which were recently proposed theoretically and shown to be free from the self-doping in Ref. [18]. By means of the strong-coupling expansion, energy mapping method, and local force approach, we found that J for these nickelates is as large as 100 meV, which is not far smaller than that of the cuprates. This result suggests that the d^9 nickelates and cuprates share a notable common feature in the Mott insulating phase, although the former and latter belong to the Mott-Hubbard and charge-transfer regimes, respectively.

Finally, we note that the proposed d^9 nickelates might give rare examples of realizing the square-lattice Hubbard model with sizable J in real materials. Recent numerical studies show that the phase diagram of the doped Hubbard model is under severe competition between the stripe state with charge/spin modulation and d-wave superconductivity [89–92]. Therefore, once synthesized, the d^9 nickelates will serve as a valuable test-bed system to understand the superconductivity in the Hubbard-like model. They are also an important reference to understand the superconducting mechanism in the cuprates, because they would tell us whether the charge-transfer nature in the cuprates is essential in the high-T_c superconductivity or not.

ACKNOWLEDGMENTS

We acknowledge financial support from JSPS KAKENHI Grants No. 16H06345 (Y.N., M.H., and R.A.), No. 17K14336 (Y.N.), No. 18H01158 (Y.N.), No. 19K14654 (T.N.), No. 19H05825 (R.A.), No. 20K14390 (M.H.), No. 20K21067 (T.N.), and No. 20K14423 (Y.N.). This work was supported by MEXT through the "Program for Promoting Researches on the Supercomputer Fugaku" (Basic Science for Emergence and Functionality in Quantum Matter). Some of the calculations were performed at Supercomputer Center, Institute for Solid State Physics, University of Tokyo.

APPENDIX: EXCHANGE COUPLING J FROM THE d-p MODEL

In the main text, we estimated J by the strong-coupling expansion starting from the single-band Hubbard model. Here we show that the J value is also on the order of 100 meV even when we perform the strong-coupling expansion based on the so-called d-p model consisting of Ni $3d_{x^2-y^2}$ and two O $2p$ orbitals. In the strong-coupling expansion of the d-p model for the filling of one hole per unit cell, J is given by

$$J = \frac{4t_{dp}^4}{\Delta_{dp}^2 U_{dd}} + \frac{4t_{dp}^4}{\Delta_{dp}^2(\Delta_{dp} + U_{pp}/2)}, \tag{A1}$$

where t_{dp} is the hopping between Ni $3d_{x^2-y^2}$ and O $2p$ orbitals and U_{dd} and U_{pp} are the on-site Coulomb repulsion for Ni $3d_{x^2-y^2}$ and O $2p$ orbitals, respectively.

Using the RESPACK [77,78] based on the cRPA method [58,93] combined with the maximally localized Wannier functions [75,76], we constructed the three-orbital d-p model from first principles. We consider the double-counting effect in the Hartree term and Δ_{dp} is given by $\Delta_{dp} = \Delta_{dp}^{\mathrm{DFT}} + U_{dd}\, n_d^{\mathrm{DFT}}/2 - U_{pp}\, n_p^{\mathrm{DFT}}/2$, where the superscript DFT stands for the DFT value and n is the hole occupation.

For $RbCa_2NiO_3$, we obtain $|t_{dp}| = 1.23$ eV, $\Delta_{dp} = 5.46$ eV ($\Delta_{dp}^{\mathrm{DFT}} = 4.11$ eV), $U_{dd} = 4.83$ eV, and $U_{pp} = 4.62$ eV. Then the J value is estimated as $J = 103$ meV.

For $A_2NiO_2Br_2$ ($A = Ba_{0.5}La_{0.5}$), we get $|t_{dp}| = 1.24$ eV, $\Delta_{dp} = 5.86$ eV ($\Delta_{dp}^{\mathrm{DFT}} = 4.37$ eV), $U_{dd} = 5.05$ eV, and $U_{pp} = 4.57$ eV. The resulting J value is $J = 88$ meV.

[1] D. Li, K. Lee, B. Y. Wang, M. Osada, S. Crossley, H. R. Lee, Y. Cui, Y. Hikita, and H. Y. Hwang, Superconductivity in an infinite-layer nickelate, Nature (London) **572**, 624 (2019).

[2] G. A. Sawatzky, Superconductivity seen in a non-magnetic nickel oxide, Nat. News Views **572**, 592 (2019).

[3] M. Hepting, D. Li, C. J. Jia, H. Lu, E. Paris, Y. Tseng, X. Feng, M. Osada, E. Been, Y. Hikita *et al.*, Electronic structure of the parent compound of superconducting infinite-layer nickelates, Nat. Mater. **19**, 381 (2020).

[4] Q. Li, C. He, J. Si, X. Zhu, Y. Zhang, and H.-H. Wen, Absence of superconductivity in bulk $Nd_{1-x}Sr_xNiO_2$, Commun. Mater. **1**, 16 (2020).

[5] X.-R. Zhou, Z.-X. Feng, P.-X. Qin, H. Yan, S. Hu, H.-X. Guo, X.-N. Wang, H.-J. Wu, X. Zhang, H.-Y. Chen, X.-P. Qiu, and Z.-Q. Liu, Absence of superconductivity in $Nd_{0.8}Sr_{0.2}NiO_x$ thin films without chemical reduction, Rare Metals **39**, 368 (2020).

[6] Y. Fu, L. Wang, H. Cheng, S. Pei, X. Zhou, J. Chen, S. Wang, R. Zhao, W. Jiang, C. Liu, M. Huang, X. Wang, Y. Zhao, D. Yu, F. Ye, S. Wang, and J.-W. Mei, Core-level x-ray photoemission and Raman spectroscopy studies on electronic structures in Mott-Hubbard type nickelate oxide $NdNiO_2$, arXiv:1911.03177.

[7] K. Lee, B. H. Goodge, D. Li, M. Osada, B. Y. Wang, Y. Cui, L. F. Kourkoutis, and H. Y. Hwang, Aspects of the synthesis of thin film superconducting infinite-layer nickelates, APL Mater. **8**, 041107 (2020).

[8] D. Li, B. Y. Wang, K. Lee, S. P. Harvey, M. Osada, B. H. Goodge, L. F. Kourkoutis, and H. Y. Hwang, Superconducting Dome in $Nd_{1-x}Sr_xNiO_2$ Infinite Layer Films, Phys. Rev. Lett. **125**, 027001 (2020).

[9] S. Zeng, C. S. Tang, X. Yin, C. Li, Z. Huang, J. Hu, W. Liu, G. J. Omar, H. Jani, Z. S. Lim, K. Han, D. Wan, P. Yang, A. T. S. Wee, and A. Ariando, Phase Diagram and Superconducting

Dome of Infinite-Layer $Nd_{1-x}Sr_xNiO_2$ Thin Films, Phys. Rev. Lett. **125**, 147003 (2020).

[10] B. H. Goodge, D. Li, M. Osada, B. Y. Wang, K. Lee, G. A. Sawatzky, H. Y. Hwang, and L. F. Kourkoutis, Doping evolution of the Mott-Hubbard landscape in infinite-layer nickelates, arXiv:2005.02847.

[11] B.-X. Wang, H. Zheng, E. Krivyakina, O. Chmaissem, P. P. Lopes, J. W. Lynn, L. C. Gallington, Y. Ren, S. Rosenkranz, J. F. Mitchell, and D. Phelan, Synthesis and characterization of bulk $Nd_{1-x}Sr_xNiO_2$ and $Nd_{1-x}Sr_xNiO_3$, Phys. Rev. Materials **4**, 084409 (2020).

[12] Q. Gu, Y. Li, S. Wan, H. Li, W. Guo, H. Yang, Q. Li, X. Zhu, X. Pan, Y. Nie, and H.-H. Wen, Two superconducting components with different symmetries in $Nd_{1-x}Sr_xNiO_2$ films, arXiv:2006.13123.

[13] M. Osada, B. Y. Wang, B. H. Goodge, K. Lee, H. Yoon, K. Sakuma, D. Li, M. Miura, L. F. Kourkoutis, and H. Y. Hwang, A superconducting praseodymium nickelate with infinite layer structure, Nano Lett. **20**, 5735 (2020).

[14] A. S. Botana and M. R. Norman, Similarities and Differences between $LaNiO_2$ and $CaCuO_2$ and Implications for Superconductivity, Phys. Rev. X **10**, 011024 (2020).

[15] H. Sakakibara, H. Usui, K. Suzuki, T. Kotani, H. Aoki, and K. Kuroki, Model Construction and a Possibility of Cupratelike Pairing in a New d^9 Nickelate Superconductor (Nd, Sr)NiO_2, Phys. Rev. Lett. **125**, 077003 (2020).

[16] J. Hirsch and F. Marsiglio, Hole superconductivity in infinite-layer nickelates, Physica C **566**, 1353534 (2019).

[17] Y. Nomura, M. Hirayama, T. Tadano, Y. Yoshimoto, K. Nakamura, and R. Arita, Formation of a two-dimensional single-component correlated electron system and band engineering in the nickelate superconductor $NdNiO_2$, Phys. Rev. B **100**, 205138 (2019).

[18] M. Hirayama, T. Tadano, Y. Nomura, and R. Arita, Materials design of dynamically stable d^9 layered nickelates, Phys. Rev. B **101**, 075107 (2020).

[19] J. Gao, Z. Wang, C. Fang, and H. Weng, Electronic structures and topological properties in nickelates $Ln_{n+1}Ni_nO_{2n+2}$, Natl. Sci. Rev. nwaa218 (2020).

[20] M. Jiang, M. Berciu, and G. A. Sawatzky, Critical Nature of the Ni Spin State in Doped $NdNiO_2$, Phys. Rev. Lett. **124**, 207004 (2020).

[21] S. Ryee, H. Yoon, T. J. Kim, M. Y. Jeong, and M. J. Han, Induced magnetic two-dimensionality by hole doping in the superconducting infinite-layer nickelate $Nd_{1-x}Sr_xNiO_2$, Phys. Rev. B **101**, 064513 (2020).

[22] H. Zhang, L. Jin, S. Wang, B. Xi, X. Shi, F. Ye, and J.-W. Mei, Effective Hamiltonian for nickelate oxides $Nd_{1-x}Sr_xNiO_2$, Phys. Rev. Research **2**, 013214 (2020).

[23] G.-M. Zhang, Y.-F. Yang, and F.-C. Zhang, Self-doped Mott insulator for parent compounds of nickelate superconductors, Phys. Rev. B **101**, 020501(R) (2020).

[24] Z. Liu, Z. Ren, W. Zhu, Z. Wang, and J. Yang, Electronic and magnetic structure of infinite-layer $NdNiO_2$: Trace of antiferromagnetic metal, npj Quantum Mater. **5**, 31 (2020).

[25] X. Wu, D. Di Sante, T. Schwemmer, W. Hanke, H. Y. Hwang, S. Raghu, and R. Thomale, Robust $d_{x^2-y^2}$-wave superconductivity of infinite-layer nickelates, Phys. Rev. B **101**, 060504(R) (2020).

[26] E. Been, W.-S. Lee, H. Y. Hwang, Y. Cui, J. Zaanen, T. Devereaux, B. Moritz, and C. Jia, Theory of rare-earth infinite layer nickelates, arXiv:2002.12300.

[27] Z.-J. Lang, R. Jiang, and W. Ku, Where do the doped hole carriers reside in the new superconducting nickelates?, arXiv:2005.00022.

[28] I. Leonov, S. L. Skornyakov, and S. Y. Savrasov, Lifshitz transition and frustration of magnetic moments in infinite-layer $NdNiO_2$ upon hole doping, Phys. Rev. B **101**, 241108(R) (2020).

[29] I. Leonov and S. Y. Savrasov, Effect of epitaxial strain on the electronic structure and magnetic correlations in infinite-layer (Nd,Sr)NiO_2, arXiv:2006.05295.

[30] P. Werner and S. Hoshino, Nickelate superconductors: Multiorbital nature and spin freezing, Phys. Rev. B **101**, 041104(R) (2020).

[31] F. Petocchi, V. Christiansson, F. Nilsson, F. Aryasetiawan, and P. Werner, Normal state of $Nd_{1-x}Sr_xNiO_2$ from self-consistent GW+EDMFT, arXiv:2006.00394.

[32] Y. Gu, S. Zhu, X. Wang, J. Hu, and H. Chen, A substantial hybridization between correlated Ni-d orbital and itinerant electrons in infinite-layer nickelates, Commun. Phys. **3**, 84 (2020).

[33] L. Si, W. Xiao, J. Kaufmann, J. M. Tomczak, Y. Lu, Z. Zhong, and K. Held, Topotactic Hydrogen in Nickelate Superconductors and Akin Infinite-Layer Oxides ABO_2, Phys. Rev. Lett. **124**, 166402 (2020).

[34] F. Lechermann, Late transition metal oxides with infinite-layer structure: Nickelates versus cuprates, Phys. Rev. B **101**, 081110(R) (2020).

[35] F. Lechermann, Multiorbital Processes Rule the $Nd_{1-x}Sr_xNiO_2$ Normal State, Phys. Rev. X **10**, 041002 (2020).

[36] J. Karp, A. S. Botana, M. R. Norman, H. Park, M. Zingl, and A. Millis, Many-Body Electronic Structure of $NdNiO_2$ and $CaCuO_2$, Phys. Rev. X **10**, 021061 (2020).

[37] M. Kitatani, L. Si, O. Janson, R. Arita, Z. Zhong, and K. Held, Nickelate superconductors—A renaissance of the one-band Hubbard model, npj Quantum Mater. **5**, 59 (2020).

[38] Y. Wang, C. J. Kang, H. Miao, and G. Kotliar, Hund's metal physics: From $SrNiO_2$ to $NdNiO_2$, arXiv:2006.15305.

[39] Y.-H. Zhang and A. Vishwanath, Type-II t-J model in superconducting nickelate $Nd_{1-x}Sr_xNiO_2$, Phys. Rev. Research **2**, 023112 (2020).

[40] L.-H. Hu and C. Wu, Two-band model for magnetism and superconductivity in nickelates, Phys. Rev. Research **1**, 032046 (2019).

[41] J. Chang, J. Zhao, and Y. Ding, Hund-Heisenberg model in superconducting infinite-layer nickelates, arXiv:1911.12731.

[42] Z. Wang, G.-M. Zhang, Y.-F. Yang, and F.-C. Zhang, Distinct pairing symmetries of superconductivity in infinite-layer nickelates, arXiv:2006.15928.

[43] P. Jiang, L. Si, Z. Liao, and Z. Zhong, Electronic structure of rare-earth infinite-layer $RNiO_2$(R = La, Nd), Phys. Rev. B **100**, 201106(R) (2019).

[44] M.-Y. Choi, K.-W. Lee, and W. E. Pickett, Role of 4f states in infinite-layer $NdNiO_2$, Phys. Rev. B **101**, 020503(R) (2020).

[45] B. Geisler and R. Pentcheva, Fundamental difference in the electronic reconstruction of infinite-layer versus perovskite neodymium nickelate films on $SrTiO_3$(001), Phys. Rev. B **102**, 020502(R) (2020).

[46] R. He, P. Jiang, Y. Lu, Y. Song, M. Chen, M. Jin, L. Shui, and Z. Zhong, Polarity-induced electronic and atomic reconstruction at $NdNiO_2/SrTiO_3$ interfaces, Phys. Rev. B **102**, 035118 (2020).

[47] F. Bernardini and A. Cano, Stability and electronic properties of $LaNiO_2/SrTiO_3$ heterostructures, J. Phys. Mater. **3**, 03LT01 (2020).

[48] F. Bernardini, V. Olevano, X. Blase, and A. Cano, Infinite-layer fluoro-nickelates as d^9 model materials, J. Phys. Mater. **3**, 035003 (2020).

[49] V. Olevano, F. Bernardini, X. Blase, and A. Cano, *Ab initio* many-body *GW* correlations in the electronic structure of $LaNiO_2$, Phys. Rev. B **101**, 161102(R) (2020).

[50] M.-Y. Choi, W. E. Pickett, and K. W. Lee, Quantum-fluctuation-frustrated flat band instabilities in $NdNiO_2$, Phys. Rev. Research **2**, 033445 (2020).

[51] P. Adhikary, S. Bandyopadhyay, T. Das, I. Dasgupta, and T. Saha-Dasgupta, Orbital selective superconductivity in a two-band model of infinite-layer nickelates, Phys. Rev. B **102**, 100501 (2020).

[52] E. M. Nica, J. Krishna, R. Yu, Q. Si, A. S. Botana, and O. Erten, Theoretical investigation of superconductivity in trilayer square-planar nickelates, Phys. Rev. B **102**, 020504 (2020).

[53] P. A. Lee, N. Nagaosa, and X.-G. Wen, Doping a Mott insulator: Physics of high-temperature superconductivity, Rev. Mod. Phys. **78**, 17 (2006).

[54] J. Zaanen, G. A. Sawatzky, and J. W. Allen, Band Gaps and Electronic Structure of Transition-Metal Compounds, Phys. Rev. Lett. **55**, 418 (1985).

[55] M. Ogata and H. Fukuyama, The t–J model for the oxide high-T_c superconductors, Rep. Prog. Phys. **71**, 036501 (2008).

[56] K.-W. Lee and W. E. Pickett, Infinite-layer $LaNiO_2$: Ni^{1+} is not Cu^{2+}, Phys. Rev. B **70**, 165109 (2004).

[57] Y. Tokura and T. Arima, New classification method for layered copper oxide compounds and its application to design of new high T_c superconductors, Jpn. J. Appl. Phys. **29**, 2388 (1990).

[58] F. Aryasetiawan, M. Imada, A. Georges, G. Kotliar, S. Biermann, and A. I. Lichtenstein, Frequency-dependent local interactions and low-energy effective models from electronic structure calculations, Phys. Rev. B **70**, 195104 (2004).

[59] A. Lichtenstein, in *Correlated Matter Modeling and Simulation*, edited by E. Pavarini, E. Koch, and U. Schollwöck (Verlag des Forschungszentrum Jülich, Jülich, 2013), Vol. 3.

[60] J. Otsuki, K. Yoshimi, H. Shinaoka, and Y. Nomura, Strong-coupling formula for momentum-dependent susceptibilities in dynamical mean-field theory, Phys. Rev. B **99**, 165134 (2019).

[61] M. Takahashi, Half-filled Hubbard model at low temperature, J. Phys. C **10**, 1289 (1977).

[62] A. H. MacDonald, S. M. Girvin, and D. Yoshioka, $\frac{t}{U}$ expansion for the Hubbard model, Phys. Rev. B **37**, 9753 (1988).

[63] J.-Y. P. Delannoy, M. J. P. Gingras, P. C. W. Holdsworth, and A.-M. S. Tremblay, Low-energy theory of the $t-t'-t''-U$ Hubbard model at half-filling: Interaction strengths in cuprate superconductors and an effective spin-only description of La_2CuO_4, Phys. Rev. B **79**, 235130 (2009).

[64] V. I. Anisimov, J. Zaanen, and O. K. Andersen, Band theory and Mott insulators: Hubbard U instead of Stoner I, Phys. Rev. B **44**, 943 (1991).

[65] V. I. Anisimov, I. V. Solovyev, M. A. Korotin, M. T. Czyżyk, and G. A. Sawatzky, Density-functional theory and NiO photoemission spectra, Phys. Rev. B **48**, 16929 (1993).

[66] A. I. Liechtenstein, V. I. Anisimov, and J. Zaanen, Density-functional theory and strong interactions: Orbital ordering in Mott-Hubbard insulators, Phys. Rev. B **52**, R5467 (1995).

[67] M. Cococcioni, in *Correlated Electrons: From Models to Materials Modeling and Simulation*, edited by E. Pavarini, E. Koch, F. Anders, and M. Jarrell (Verlag des Forschungszentrum Jülich, Jülich, 2012), Vol. 2.

[68] D. M. Korotin, V. V. Mazurenko, V. I. Anisimov, and S. V. Streltsov, Calculation of exchange constants of the Heisenberg model in plane-wave-based methods using the Green's function approach, Phys. Rev. B **91**, 224405 (2015).

[69] T. Nomoto, T. Koretsune, and R. Arita, Local force method for the *ab initio* tight-binding model: Effect of spin-dependent hopping on exchange interactions, Phys. Rev. B **102**, 014444 (2020).

[70] T. Nomoto, T. Koretsune, and R. Arita, Formation Mechanism of Helical Q Structure in Gd-Based Skyrmion Materials, Phys. Rev. Lett. **125**, 117204 (2020).

[71] P. Giannozzi, O. Andreussi, T. Brumme, O. Bunau, M. B. Nardelli, M. Calandra, R. Car, C. Cavazzoni, D. Ceresoli, M. Cococcioni *et al.*, Advanced capabilities for materials modeling with QUANTUM ESPRESSO, J. Phys.: Condens. Matter **29**, 465901 (2017).

[72] J. P. Perdew, K. Burke, and M. Ernzerhof, Generalized Gradient Approximation Made Simple, Phys. Rev. Lett. **77**, 3865 (1996).

[73] M. J. van Setten, M. Giantomassi, E. Bousquet, M. J. Verstraete, D. R. Hamann, X. Gonze, and G.-M. Rignanese, The PSEUDODOJO: Training and grading a 85 element optimized norm-conserving pseudopotential table, Comput. Phys. Commun. **226**, 39 (2018).

[74] D. R. Hamann, Optimized norm-conserving Vanderbilt pseudopotentials, Phys. Rev. B **88**, 085117 (2013).

[75] N. Marzari and D. Vanderbilt, Maximally localized generalized Wannier functions for composite energy bands, Phys. Rev. B **56**, 12847 (1997).

[76] I. Souza, N. Marzari, and D. Vanderbilt, Maximally localized Wannier functions for entangled energy bands, Phys. Rev. B **65**, 035109 (2001).

[77] K. Nakamura, Y. Yoshimoto, Y. Nomura, T. Tadano, M. Kawamura, T. Kosugi, K. Yoshimi, T. Misawa, and Y. Motoyama, RESPACK: An ab initio tool for derivation of effective low-energy model of material, arXiv:2001.02351.

[78] https://sites.google.com/view/kazuma7k6r

[79] H. Shinaoka, J. Otsuki, M. Ohzeki, and K. Yoshimi, Compressing Green's function using intermediate representation between imaginary-time and real-frequency domains, Phys. Rev. B **96**, 035147 (2017).

[80] N. Chikano, K. Yoshimi, J. Otsuki, and H. Shinaoka, irbasis: Open-source database and software for intermediate-representation basis functions of imaginary-time Green's function, Comput. Phys. Commun. **240**, 181 (2019).

[81] J. Li, M. Wallerberger, N. Chikano, C.-N. Yeh, E. Gull, and H. Shinaoka, Sparse sampling approach to efficient *ab initio* calculations at finite temperature, Phys. Rev. B **101**, 035144 (2020).

[82] K. B. Lyons, P. A. Fleury, J. P. Remeika, A. S. Cooper, and T. J. Negran, Dynamics of spin fluctuations in lanthanum cuprate, Phys. Rev. B **37**, 2353 (1988).

[83] K. B. Lyons, P. A. Fleury, L. F. Schneemeyer, and J. V. Waszczak, Spin Fluctuations and Superconductivity in $Ba_2YCu_3O_{6+\delta}$, Phys. Rev. Lett. **60**, 732 (1988).

[84] S. Sugai, S.-i. Shamoto, and M. Sato, Two-magnon Raman scattering in $(La_{1-x}Sr_x)_2CuO_4$, Phys. Rev. B **38**, 6436 (1988).

[85] R. R. P. Singh, P. A. Fleury, K. B. Lyons, and P. E. Sulewski, Quantitative Determination of Quantum Fluctuations in the Spin-1/2 Planar Antiferromagnet, Phys. Rev. Lett. **62**, 2736 (1989).

[86] P. E. Sulewski, P. A. Fleury, K. B. Lyons, S.-W. Cheong, and Z. Fisk, Light scattering from quantum spin fluctuations in R_2CuO_4 (R=La, Nd, Sm), Phys. Rev. B **41**, 225 (1990).

[87] Y. Tokura, S. Koshihara, T. Arima, H. Takagi, S. Ishibashi, T. Ido, and S. Uchida, Cu-O network dependence of optical charge-transfer gaps and spin-pair excitations in single-CuO_2-layer compounds, Phys. Rev. B **41**, 11657 (1990).

[88] M. S. Hybertsen, E. B. Stechel, M. Schluter, and D. R. Jennison, Renormalization from density-functional theory to strong-coupling models for electronic states in Cu-O materials, Phys. Rev. B **41**, 11068 (1990).

[89] B.-X. Zheng, C.-M. Chung, P. Corboz, G. Ehlers, M.-P. Qin, R. M. Noack, H. Shi, S. R. White, S. Zhang, and G. K.-L. Chan, Stripe order in the underdoped region of the two-dimensional Hubbard model, Science **358**, 1155 (2017).

[90] A. S. Darmawan, Y. Nomura, Y. Yamaji, and M. Imada, Stripe and superconducting order competing in the Hubbard model on a square lattice studied by a combined variational Monte Carlo and tensor network method, Phys. Rev. B **98**, 205132 (2018).

[91] T. Ohgoe, M. Hirayama, T. Misawa, K. Ido, Y. Yamaji, and M. Imada, *Ab initio* study of superconductivity and inhomogeneity in a Hg-based cuprate superconductor, Phys. Rev. B **101**, 045124 (2020).

[92] H.-C. Jiang and T. P. Devereaux, Superconductivity in the doped Hubbard model and its interplay with next-nearest hopping t', Science **365**, 1424 (2019).

[93] E. Şaşıoğlu, C. Friedrich, and S. Blügel, Effective Coulomb interaction in transition metals from constrained random-phase approximation, Phys. Rev. B **83**, 121101(R) (2011).